Measurement report: On the contribution of long-distance transport to the secondary aerosol formation and aging

Haobin Zhong[1,2], Ru-Jin Huang[1,2,3], Chunshui Lin[1], Wei Xu[1], Jing Duan[1], Yifang Gu[1,2], Wei Huang[1], Haiyan Ni[1], Chongshu Zhu[1], Yan You[4], Yunfei Wu[5], Renjian Zhang[5], Jurgita Ovadnevaite[6], Darius Ceburnis[6], Colin D. O'Dowd[6]

[1]State Key Laboratory of Loess and Quaternary Geology (SKLLQG), Center for Excellence in Quaternary Science and Global Change, and Key Laboratory of Aerosol Chemistry and Physics, Institute of Earth Environment, Chinese Academy of Sciences, Xi'an 710061, China

[2]University of Chinese Academy of Sciences, Beijing 100049, China

[3]Open Studio for Oceanic-Continental Climate and Environment Changes, Pilot National Laboratory for Marine Science and Technology (Qingdao), 266061 Qingdao, China

[4]National Observation and Research Station of Coastal Ecological Environments in Macao, Macao Environmental Research Institute, Macau University of Science and Technology, Macao SAR 999078, China

[5]Key Laboratory of Middle Atmosphere and Global Environment Observation (LAGEO), Institute of Atmospheric Physics, Chinese Academy of Sciences, Beijing 100029, China

[6]School of Physics and Ryan Institute's Centre for Climate & Air Pollution Studies, National University of Ireland Galway, University Road, Galway H91CF50, Ireland

Correspondence to: Ru-Jin Huang (rujin.huang@ieecas.cn)

Abstract

To investigate the physio-chemical properties of aerosol transported from major pollution regions in China, observations were conducted ~200 m above the ground at the junction location of the North China Plain and Fenwei Basin, which are two regions of top priority for China's blue sky campaign. We identified three pollution transport sectors including those from Beijing-Tianjin-Hebei (BTH), urban Guanzhong Basin (GZB), northern China and one clean transport sector from rural Guanzhong Basin region. Secondary inorganic aerosol (SIA) constituted a major fraction (39-46%) in all pollution transport sectors with high sulphur oxidation ratio (0.44-0.58) and nitrogen oxidation ratio (0.24-0.29), suggesting efficient formation of secondary inorganic aerosol during regional transport. While more oxidized oxygenated organic aerosol (MO-OOA) played a dominant role in the source of organic aerosol in all sectors including the clean one, accounting for 42-58% of total organic aerosol. Elemental analysis (O and C) shows that aerosol particles at this receptor site were much more oxidized than urban regions, pointing that long-range transport contributed markedly to the organic aerosol oxidation and aging. Case studies of pollution events with high sulphate, nitrate and more-oxidized oxygenated organic aerosol production rate indicate the strong formation efficiency of secondary aerosol during regional transport in the Beijing-Tianjin-Hebei

transport sector.

Keywords: Regional transport; Secondary aerosol formation; More oxidized organic aerosol; Air pollution.

1 Introduction

Air pollution events with high levels of fine particles (particulate matter with a diameter ≤ 2.5 μm, $PM_{2.5}$) were frequently occurred in China over the past years, due to rapid industrialization and urbanization (Lelieveld et al., 2015; Feng et al., 2018; An et al., 2019). The high level of $PM_{2.5}$ affects air quality, human health and climate, thus, has received widespread concerns around the world (Tie et al., 2016; Cohen et al., 2017). To better understand air pollution in China, many field studies has been carried out in the last decades (Tie et al., 2009; Lei et al., 2011; Cao et al., 2012; Huang et al., 2014; Liu et al., 2018). Most of these studies for particle properties are based on local observations, such as in Beijing (Sun et al., 2013; Li et al., 2019), Shanghai (Xu et al., 2012; Huang et al., 2013; Wang et al., 2020), Xi'an (Huang et al., 2014; Duan et al., 2021; Lin et al., 2022), Guangzhou (Guo et al., 2020; Chen et al., 2021), and Hong Kong (Li et al., 2015; Sun et al., 2016). However, aerosol particles can affect hundreds of kilometers through transport depending on particle size and chemical compositions (Uno et al., 2009). During transport, aerosols undergo further transformation, altering chemical composition and oxidation level and consequently affecting their chemo-physical properties and climate impact (Moffet and Prather, 2009; Riemer and West, 2013; Calvo et al., 2013; Fierce et al., 2016).

Recent studies found that local formation cannot fully explain the increase of SIA during pollution events, and the regional transport was considered as an important source for the increase of SIA (Yang et al., 2015; Tang et al., 2016). Some modeling studies reported that heterogeneous chemistry during the transport was identified as the dominant factor during haze episodes in mega cities (Li and Han, 2016; Li et al., 2017), and were further supported by the observations. Du et al. (2019) reported that the chemical transformation from SO_2 to sulphate was the major source of sulphate in Beijing. Li et al. (2021) suggested that the pollution in winter in Beijing was largely affected by the regional transport, and the water vapor during the transport of the air mass greatly increased SIA proportion. Gunsch et al. (2018) claimed that the particles were heavily coated with SOA formed during the transport, with 89% of organics fractions in PM_1 and 0.8 O/C ratio in the forested Great Lakes region during wild-fire period. Most of the existing studies were devoted to studying the contribution of regional transport to pollution events in urban areas, while the study on region-to-region transport was limited. Our previous study reported that different regions in China represented different chemical compositions and OA sources due to different types of emission characteristics (Zhong et al., 2020). Therefore, the transport aerosol particles from different regions may have completely different properties due to different precursors and transport conditions. The study of region-to-region transport can provide insight to the interactions and mixing properties of particles on a national scale.

Investigation of the chemical compositions and sources with the transport pathways in background areas is a common method to understand the influence of long-distance transport

of aerosol on the atmospheric environment (Schichtel et al., 2006; Salvador et al., 2008; Das and Jayaraman, 2012; Tang et al., 2014; Pu et al., 2015). In this study, we performed a one-month observation at a regional receptor site to investigate the characteristics of aerosol transported from the major pollution regions by using a time-of-flight aerosol chemical speciation monitor (TOF-ACSM). The receptor site is geographically located in the middle part of China, at the junction of the BTH region and the GZB region, which are the two of the three key regions in Protection of Blue Sky issued by the National Congress for pollution control and sustainable development in 2018. In addition, the chemical composition of non-refractory $PM_{2.5}$ (organics, sulphate, nitrate, ammonium, and chloride) and OA source apportionment were resolved and analyzed with measured black carbon, gas-phase pollutants (SO_2, CO, NO_2 and O_3) and meteorological parameters to provide complementary mass-based characterization of the transported aerosols.

2 Experimental

2.1 Sampling site and instrumentation

The sampling was carried out on the rooftop of Le Méridien hotel, which was a 33-floor tall building and about 200 meter above the ground (34.34°N, 109.02°E), during summer from 19th May to 18th June 2018. It is located in the central area of Chan-ba Ecological District (CBE, 129 km^2), which was a new ecological district, located at the eastern part of the GZB region. The sampling site was surrounded by wetlands and lawns.

A TOF-ACSM (Aerodyne Research Inc., Billerica, MA) was deployed in an air-conditioned room on the top floor (32^{nd}) of Le Méridien hotel for continuous on-line measurements of non-refractory $PM_{2.5}$ species including organics (Org), sulphate (SO_4^{2-}), nitrate (NO_3^-), ammonium (NH_4^+), and chloride (Cl^-). The sampling time resolution was 5 minutes. Also, a scanning mobility particles sizer with a differential mobility analyzer (DMA, model 3080) and a condensation particle counter (CPC, model 3772) (TSI Incorporated, Shoreview, Minnesota, USA) were combined for the particle number size distribution measurement between 10 ~ 840 nm, which shared an inlet with TOF-ACSM through a $PM_{2.5}$ cyclone (URG-2000-30ED, URG Corp., Chapel Hill, NC). Black carbon concentration was measured by an aethalometer (AE33, Magee Scientific) through an individual $PM_{2.5}$ cyclone (SCC, BGI) inlet. The sampling time-resolution was 1 min at a flow rate of 5 L min^{-1}. Gas-phase pollutants (SO_2, CO, NO, NO_2 and O_3) were measured by the gas analyzers (Thermo Scientific Inc.). Meteorological data (temperature, RH, wind speed and wind direction) were measured by an automatic weather station (MAWS201, Vaisala, Vantaa, Finland) and a wind sensor (Vaisala Model QMW101-M2). All ambient inlets of instruments were set on the rooftop (33^{rd}, 200 m) and were 1.5 m in height.

2.2 TOF-ACSM operation

TOF-ACSM has been detailed previously (Fröhlich et al., 2013). Briefly, ambient air was sampled through a $PM_{2.5}$ cyclone and a 3/8-inch polished stainless-steel tube (Swagelok company, Solon, OH) with a constant flow rate of 3 L min^{-1} (0.3 L min^{-1} for SMPS and CPC, 0.08 L min^{-1} for TOF-ACSM and 2.62 L min^{-1} for an extra constant flow air pump) for the

coarse particles cut. Following that, particles were focused into a narrow particle beam via a $PM_{2.5}$ aerodynamic lens. Then the particles were evaporated by a thermal standard vaporizer (~ 600ºC) and ionized by an electron impact ionization (70eV), and the resulting ion fragments were analyzed and determined by a time-of-flight mass spectrometer. Also, a Nafion dryer was used to remove moisture prior to entering TOF-ACSM and SMPS, which kept the relative humidity (RH) of the particle beam under 30%. Meanwhile, an automatically switching valve was installed on the main air path between the Nafion dryer and TOF-ACSM, which was set to change the sampling flow to a high-efficiency particulate air filter for the detection limits measurement during the acquisition.

Ionization efficiency (IE) and relative ionization efficiency (RIE) calibrations were performed about every ~10 days during the campaign. Briefly, pure ammonium nitrate and ammonium sulphate particles were successively atomized by a TSI 3076 atomizer (TSI Incorporated, Shoreview, Minnesota, USA). After that, they were dried by a hollow silica gel drying tube before being imported into SMPS for 300 nm size selection, and then were counted and measured by CPC and TOF-ACSM simultaneously. The other parameter calibrations, such as the mass, the baseline, and the single ions were conducted every 3 days.

2.3 Data analysis

The chemical compositions and mass concentrations of $PM_{2.5}$ were analyzed by Tofware (v2.5.13, Tofwerk AG). Organics, nitrate and chloride were analyzed with RIEs of 1.4, 1.1 and 1.3, respectively (Canagaratna et al*.,* 2007). RIEs of ammonium and sulphate were estimated from the averaged results of IE and RIE calibration (4.7 for RIE of ammonium; 0.67 for RIE of sulphate). Besides, a particle collection efficiency (CE) for particle bounce losses was calculated as a value of 0.5, with a slight adjustment of CE value was based on a composition dependent collection efficiency (CDCE) approach following Middlebrook et al*.,* 2012. The resulting mass concentrations of chemicals of $PM_{2.5}$ were well correlated with the mass concentrations of water-soluble inorganic aerosol from our In-situ Gas and Aerosol Compositions monitor (IGAC, S-611, MachineShop) measurement (Fig. S2), suggesting the reliability of TOF-ACSM results analysis.

The OA source apportionment was performed by positive matrix factorization (PMF, Paatero and Tapper, 1994; Paatero, 1997) and multilinear engine (ME-2, Paatero, 1999). Organic aerosol matrices (data matrix, error matrix, minimum values, time series and m/z from 12~120 amus in our case) were exported from Tofware, and were resolved for source apportionment in PMF-ME-2 Toolkit SoFi (version 6.3, Canonaco et al, 2013). The optimal factor-selection and constraining strategies of SoFi were described by Elser et al. (2016). The details are presented in section S1 of the supplementary.

2.4 Trajectory analysis

The trajectory analysis was performed using the HYSPLIT model (Draxler and Hess, 1998) in Hybrid Single-Particle Lagrangian Integrated Trajectory (HYSPLIT_4). Briefly, trajectories were calculated every one hour from the air mass data which were downloaded from the National Oceanic and Atmospheric Administration (NOAA,

ftp://arlftp.arlhq.noaa.gov/pub/archives/gdas1) with 48 hours backward at a height of 200 m. The trajectories were further clustered using in TrajStat (TrajStat_v1.2).

2.5 Sulphur oxidation ratio and nitrate oxidation ratio

Sulphur oxidation ratio (SOR) and nitrate oxidation ratio (NOR) are the ratios of sulphate and nitrate to their gaseous precursors, which were widely used to represent the degree of gas-to-particle conversions of sulphur and nitrogen. SOR and NOR are calculated by solving Eq. (1) and (2) (Ji et al., 2018; Chang et al., 2020).

$$SOR = n[SO_4^{2-}]/(n[SO_4^{2-}] + n[SO_2]) \quad (1)$$

$$NOR = n[NO_3^-]/(n[NO_3^-] + n[NO_2]) \quad (2)$$

3 Results and discussion

3.1 Overview of the chemical composition, OA sources and regional transport in the receptor site

The observational site with an altitude of ~200m above the ground provides ideal to investigate the impact of regional transport on aerosol properties. Figure 1 shows an overview of the time series of the chemical components of NR-$PM_{2.5}$ (Organic, sulphate, nitrate, ammonium and chloride), together with meteorological parameters and gas-phase pollutants (SO_2, CO, NO_2 and O_3).The average mass concentration of NR-$PM_{2.5}$ was 21.5±14.9 μg m^{-3}, similar to the previous AMS/ACSM results in the western China (24.5 μg m^{-3}, Xu et al., 2014) and the southeastern China during summer (14.5-32.9 μg m^{-3}, Huang et al., 2012; Lee et al., 2013; Huang et al., 2013) but was lower than that in the northern China (41-80 μg m^{-3} , Hu et al., 2013; Duan et al., 2020). Organics constituted the largest fraction of NR-$PM_{2.5}$ (35% or 7.5 μg m^{-3}), followed by sulphate (25% or 5.3 μg m^{-3}), nitrate (17.0% or 3.7 μg m^{-3}), ammonium (14% or 3.0 μg m^{-3}), BC (8% or 1.7 μg m^{-3}), and chloride (1%, 0.2 μg m^{-3}).

Figure 2 shows the results of winds field map, cluster-averaged backward trajectory and winds rose analyses. Four transport sectors were identified, including the Beijing-Tianjin-Hebei region (BTH, the east cluster, red), the northern China (the north cluster, magenta), the rural Guanzhong Basin region (GZB, the south cluster, green) and the urban GZB region (the west cluster, blue).

The BTH transport was featured by the long-distance air mass trajectories advected over the North China Plain with an average wind speed of 1.9±1.8 m s^{-1}. The BTH transport sector accounted for 7% of the total observation days. It showed the highest mass concentration of $PM_{2.5}$ (32.9±17.4 μg m^{-3}).

The northern China transport sector was clustered by the transport from the Mongolia and the northern part of China, including Inner Mongolia and northern Shaanxi province. It represented the longest transport distance with an average wind speed of 2.2±2.1 m s^{-1} and accounted for 22% of observation days. The $PM_{2.5}$ mass in the northern China transport sector was 24.9±12.9 μg m^{-3}, which was lower than that in the BTH transport sector.

The urban GZB transport sector was from the west of the GZB region, including those large cities in the GZB region, such as Baoji, Xianyang and Xi'an. The urban GZB transport sector was the most frequent pathway during the campaign, accounting for 60% of observation days with an average wind speed of 1.0±0.9 m s^{-1}. The $PM_{2.5}$ mass in the urban GZB transport sector was 21.7±14.8 μg m^{-3}. Finally, the rural GZB transport sector mainly consisted of the air mass from Mt. Qinling, representing the air mass with least anthropogenic influence and accounting for 11% of observation days with an average wind speed of 1.9±0.7 m s^{-1} and the lowest average $PM_{2.5}$ mass (8.8±5.5 μg m^{-3}).

3.2 Secondary inorganic formation during the transport

Figure 3 shows the mass concentrations of the measured components, their fractional contributions, the sulphur oxidation ratio (SOR) and the nitrogen oxidation ratio (NOR) in these four transport sectors. SIA showed the highest mass concentration of 21.4±11.9 μg m^{-3} in the BTH transport sector, followed by the northern China transport sector (15.2±6.6 μg m^{-3}), the urban GZB transport sector (12.2±3.1 μg m^{-3}) and the rural GZB transport sector (3.5±1.7 μg m^{-3}). The corresponding fractional contributions of SIA to $PM_{2.5}$ were 64%, 60%, 55%, and 39%. The difference in SIA mass and fractional contributions suggests the difference in SIA precursor concentrations (i.e., SO_2, NO_X and NH_3) and SIA formation efficiency among different transport sectors, as discussed below.

Sulphate was the dominant fraction in the BTH transport sector, accounting for 30% of $PM_{2.5}$. This fraction decreased to 25% and 24% in the northern China transport sector and the urban GZB transport sector, respectively. Nitrate showed no obvious difference in the three urban transport sectors, accounting for 17-19% of $PM_{2.5}$. For the rural GZB transport sector, the fraction of sulphate and nitrate largely decreased to 19% and 11% of $PM_{2.5}$ respectively, consistent with lower SO_2 (3.2±2.5 μg m^{-3}) and NO_2 (27.8±10.3 μg m^{-3}) in the rural GZB transport sector which was about half of that in the three urban transport sectors (6.3-7.3 μg m^{-3} for SO_2 and 44.7-51.3 μg m^{-3} for NO_2). High fraction of sulphate in the BTH transport sector was supported by high concentrations of SO_2 and sulphate in the BTH region and central China region (Du et al., 2019; Chen et al., 2020; Li et al., 2021; Sun et al., 2022). It was further supported by high sulphur conversion efficiency (SOR), for which the BTH transport sector showed the highest SOR of 0.58, followed by the northern China transport sector (0.52), the urban GZB transport sector (0.49), and the rural GZB transport sector (0.44) (Figure 3c). Similarly, NOR showed relatively high value of 0.29 in the BTH transport sector and the northern China transport sector, and was slightly low in the urban GZB transport sector (0.25) and the rural GZB transport sector (0.24), consistent with high nitrate fraction in the BTH transport sector and the northern China sector (Figure 3d). In comparison with the previously reported results which were investigated in the source regions of the urban GZB transport sector and the BTH transport sector (Xu et al., 2019; Duan et al., 2021), SOR and NOR showed obvious increase after transport. For SOR it increased from 0.36 to 0.44 in the urban GZB transport pathway and from 0.53 to 0.58 in the BTH transport pathway, while for NOR it increased from 0.06 to 0.25 in the urban GZB transport pathway and from 0.15 to 0.29 in the BTH transport pathway. The increases in SOR and NOR after transport suggest the efficient sulphate and nitrate formation during the regional transport. This was also reflected in the

sulphate and nitrate fractions (Figure 4). After transport the fractional contribution of sulphate increased from 17% (3.8 μg m^{-3}) to 26% (5.6 μg m^{-3}) in the urban GZB transport pathway and from 20% (6.2 μg m^{-3}) to 32% (9.9 μg m^{-3}) in the BTH transport pathway, while the nitrate fraction increased from 12% (2.7 μg m^{-3}) to 19% (3.7 μg m^{-3}) in the urban GZB transport pathway but slightly decreased from 24% (7.4 μg m^{-3}) to 19% (5.9 μg m^{-3}) in the BTH transport pathway likely due to the mass loss of semi-volatile aerosol species (such as NH_4NO_3) when aerosols are exposed to a cleaner environment during the long-distance transport (Liu et al., 2021). We also compared the pollution episodes caused by the continuous transport from the BTH (EP1) and the urban GZB (EP2) (as shown in the shaded area in Figure 1, detailed in Fig. S3). Sulphate and nitrate were normalized by BC to minimize the influence of primary emission or dilution (Figure 5). Sulphate/BC ratio increased with the transport in both EP1 and EP2, with a growth rate of 0.26 hr^{-1} during EP1 (increased from 1.2 to 9.4 in 31 hours) and of 0.1 hr^{-1} during EP2 (increased from 2.3 to 16.2 in 131 hours). Nitrate/BC ratio showed a growth rate of 0.17 hr^{-1} during EP1 (increased from 1.3 to 6.6 in 31 hours) and of 5.7 times lower during EP2 (0.03 hr^{-1}, increased from 1.1 to 4.7 in 131 hours). The comparison of these two episodes further supports stronger formation of SIA in the BTH transport sector. The difference in the formation efficiency of sulphate and nitrate in different transport air masses may be related to RH, because aqueous-phase oxidation was an important formation pathway for sulphate at high RH condition (Cheng et al., 2016; Xue et al., 2019; Chang et al., 2020) and high RH also strengthened the conversion of gas-phase NH_4NO_3 to particle phase (Huang et al., 2020), which likely leads to high SOR and NOR in the BTH transport sector (81±17% of average RH).

3.3 Secondary organic formation during the transport

Figure 6 shows the mass concentrations of the resolved OA factors, their fractional contributions, the *f*44 versus *f*43 ratio and O/C ratio in these four transport sectors. *f*44/*f*43 ratio and O/C ratio are important indicators of the oxidation state of bulk OA (Ng et al., 2010), which were widely used in previous studies for SOA oxidation analysis (Xu et al., 2014; Canonaco et al., 2015; Reyes-Villegas et al., 2016). The BTH transport sector showed the highest OA mass concentration of 8.9±5.1 μg m^{-3}, followed by the urban GZB transport sector (7.3±4.0 μg m^{-3}), the northern China transport sector (6.9±3.9 μg m^{-3}) and the rural GZB transport sector (4.6± 2.5 μg m^{-3}). The corresponding fractional contributions of MO-OOA to total OA were 58% (5.2 μg m^{-3}), 55% (4.0 μg m^{-3}), 57% (4.0 μg m^{-3}), and 42% (1.9 μg m^{-3}), constituting the major OA source in the four transport sectors. The LO-OOA fraction was higher in the rural GZB transport sector (34%, 1.9 μg m^{-3}) compared to the other three urban transport sectors (around 23%, 3.9-5.2 μg m^{-3}), suggesting that SOA was less oxidized in the rural transport sector. The northern China transport sector showed the highest *f*44/*f*43 ratio of 2.1 and O/C ratio of 0.87, followed by the BTH transport sector (1.9 and 0.78), the urban GZB transport sector (1.8 and 0.72), and much lower values in the rural GZB transport sector (1.6 and 0.58). The higher *f*44/*f*43 and O/C ratio in the northern China transport sector and the BTH transport sector suggests sufficient OA aging during long-range transport. The *f*44/*f*43 ratios in these four transport sectors were higher than those in the urban sites in previous studies (triangle in Figure 6c, Ng et al., 2011) and the O/C ratios in these four transport sectors (0.72-0.87) were also much higher than those measured in urban sites in China during summer, such as Lanzhou (0.33, Xu et al., 2014) and

Jiaxing (0.28, Huang et al., 2013), but similar to the results from the mountainous site in North China Plain during summer (0.75, Li et al., 2021) and the long-range transport study in the United States (0.8, Gunsch et al., 2018). Note that the O/C ratios in the transport sectors were also much higher than those measured in the source regions of the urban GZB transport sector and the BTH transport sector, with O/C ratio increasing from 0.54 to 0.78 in the BTH transport pathway and from 0.58 to 0.72 in the urban GZB transport pathway after transport. The corresponding MO-OOA to SOA fraction also increased from 37% (3.4 μg m^{-3}) to 72% (5.2 μg m^{-3}) in the BTH transport pathway and from 37% (3.6 μg m^{-3}) to 70% (4.0 μg m^{-3}) in the urban GZB transport pathway (Figure 7), suggesting regional transport enhanced OA aging process and thus the OA oxidation state. The growth rates of MO-OOA and LO-OOA during the pollution episodes of EP1 and EP2 are shown in Figure 8. Similar to SIA, MO-OOA/BC ratio increased with the transport duration for both episodes. It showed a growth rate of 0.15 hr^{-1} during EP1 (increased from 0.23 to 4.77 in 31 hours) and of 0.06 hr^{-1} during EP2 (increased from 1.58 to 9.59 in 131 hours), suggesting stronger formation of MO-OOA in the BTH transport sector. On the contrary, LO-OOA showed no obvious increasing trend with the transport duration during EP1 and EP2, likely due to a higher conversion efficiency from LO-OOA to MO-OOA.

4. Conclusion

The observation at ~200 m above the ground in the junction of North China Plain and Fenwei Basin showed that the fraction of SIA and MO-OOA increased significantly after transport. The sulfur oxidation rate (SOR, 0.49-0.58), nitrogen oxidation rate (NOR, 0.25-0.29), $f44/f43$ ratio (1.6-2.1) and O/C ratio (0.72-0.87) were significantly higher than those investigated locally, indicating that long-distance transport largely enhanced the SIA formation, the OA oxidation and aging. The formation rate of sulphate, nitrate and MO-OOA in the BTH transport sector was much higher than that in the GZB transport sector, indicating the stronger sulphate, nitrate and MO-OOA formation efficiency in the BTH transport sector.

5. Data availability

The detailed data can be obtained from https://doi.org/10.5281/zenodo.6446514 (Zhong et al., 2022).

Acknowledgement

This work was supported by the National Natural Science Foundation of China (NSFC) under Grant No. 41925015 and 41877408, the Chinese Academy of Sciences (no. ZDBS-LY-DQC001), and the Cross Innovative Team fund from the State Key Laboratory of Loess and Quaternary Geology (No. SKLLQGTD1801).

Author contributions

Haobin Zhong: Methodology, data curation, Formal analysis, Writing – original draft, Writing – review & editing. **Ru-jin Huang**: Conceptualization, Validation, Data curation, Writing – original draft, Writing – review & editing, Supervision, Project administration, Funding

acquisition. **Chunshui Lin**: Writing - review & editing. **Wei Xu**: Writing - review & editing. **Jing Duan**: Writing - review & editing. **Yifang Gu**: Writing - review & editing. **Wei Huang**: Writing - review & editing. **Haiyan Ni**: Writing - review & editing. **Chongshu Zhu**: Resources. **Yan You**: Writing - review & editing. **Yunfei Wu**: Resources. **Renjian Zhang**: Resources. **Jurgita Ovadnevaite**: Writing - review & editing. **Darius Ceburnis**: Writing - review & editing. **Colin D. O'Dowd**: Writing - review & editing.

Competing interests

The authors have no competing interests to declare.

Reference

An, Z., Huang, R., Zhang, R., Tie, X., Li, G., Cao, J., Zhou, W., Shi, Z., Han, Y., Gu, Z., Ji, Y.: Severe haze in northern China: A synergy of anthropogenic emissions and atmospheric processes. Proc. Natl. Acad. Sci. 116, 8657–8666, 2019.

Braun, R., Aghdam, M., Bañaga, P., Betito, G., Cambaliza, M., Cruz, M., Lorenzo, G., MacDonald, A., Simpas, J., Stahl, C., Sorooshian, A.: Long-range aerosol transport and impacts on size-resolved aerosol composition in Metro Manila, Philippines. Atmos. Chem. Phys., 20, 2387–2405, 2020.

Canagaratna, M., Jayne, J., Jimenez, J., Allan, J., Alfarra, M., Zhang, Q., Onasch, T., Drewnick, F., Coe, H., Middlebrook, A., Delia, A., Williams, L., Trimborn, A., Northway, M., DeCarlo, P., Kolb, C., Davidovits, P., and Worsnop, D.: Chemical and microphysical characterization of ambient aerosols with the Aerodyne aerosol mass spectrometer, Mass Spectrom. Rev. 26(2), 185–222, 2007.

Canonaco, F., Crippa, M., Slowik, J., Baltensperger, U., and Prévôt, A.: SoFi, an Igor based interface for the efficient use of the generalized multilinear engine (ME-2) for source apportionment: application to aerosol mass spectrometer data. Atmos. Meas. Tech. 6(12), 3649-3661, 2013.

Canonaco, F., Slowik, J. G., Baltensperger, U., and Prévôt, A. S. H.: Seasonal differences in oxygenated organic aerosol composition: implications for emissions sources and factor analysis, Atmos. Chem. Phys., 15, 6993–7002, 2015.

Cao, J., Wang, Q., Chow, J., Watson, J., Tie, X., Shen, Z., Wang, P., An, Z.: Impacts of aerosol compositions on visibility impairment in Xi'an, China. Atmos. Environ. 59, 559-566, 2012.

Calvo, A., Alves, C., Castro, A., Pont, V., Vicente, A., and Fraile, R.: Research on aerosol sources and chemical composition: past, current and emerging issues, Atmos. Res., 120, 1–28, 2013.

Chang, Y., Huang, R.-J., Ge, X., Huang, X., Hu, J., Duan, Y., Zou, Z., Liu, X., and Lehmann. M.F.: Puzzling haze events in China during the coronavirus (COVID-19) shutdown. GEOPHYS. RES. LETT. 47(12), e2020GL088533, 2020.

354 Chen, T., Liu, J., Liu, Y., Ma, Q., Ge, Y., Zhong, C., Jiang, H., Chu, B., Zhang, P., Ma, J., Liu,
355 P., Wang, Y., Mu, Y., He, H.: Chemical characterization of submicron aerosol in summertime
356 Beijing: A case study in southern suburbs in 2018. Chemosphere. 247, 125918, 2020.

357 Chen, W., Ye, Y., Hu, W., Zhou, H., Pan, T., Wang, Y., Song, W., Song, Q., Ye, C., Wang, C.,
358 Wang, B., Huang, S., Yuan, B., Zhu, M., Lian, X., Zhang, G., Bi, X., Jiang, F., Liu, J.,
359 Canonaco, F., Prévôt, A., Shao, M., Wang, X.: Real-time characterization of aerosol
360 compositions, sources, and aging processes in Guangzhou during PRIDE-GBA 2018
361 campaign. Journal of Geophysical Research: Atmospheres, 126, e2021JD035114, 2021.

362 Cheng, Y., Zheng, G., Wei, C., Mu, Q., Zheng, B., Wang, Z., Gao, M., Zhang, Q., He, K.,
363 Carmichael, G., Poschl, U., Su, H.: Reactive nitrogen chemistry in aerosol water as a source
364 of sulfate during haze events in China. Sci. Adv.,2(12), e1601530, 2016.

365 Cohen, A., Brauer, M., Burnett, R., Anderson, H., Frostad, J., Estep, K., Balakrishnan, K.,
366 Brunekreef, B., Dandona, L., Dandona, R., Feigin, V., Freedman, G., Hubbell, B., Jobling,
367 A., Kan, H., Knibbs, L., Liu, Y., Martin, R., Morawska, L., Pope III, C., Shin, H., Straif, K.,
368 Shaddick, G., Thomas, M., van Dingenen, R., van Donkelaar, A., Vos, T., Murray, C., and
369 Forouzanfar, M.: Estimates and 25-year trends of the global burden of disease attributable to
370 ambient air pollution: an analysis of data from the Global Burden of Diseases Study 2015.
371 The Lancet, 389(10082), 1907 –1918, 2017.

372 Das, S. and Jayaraman, A.: Long-range transportation of anthropogenic aerosols over eastern
373 coastal region of India: investigation of sources and impact on regional climate change.
374 Atmos. Res., 118, 68-83, 2012.

375 DeCarlo, P., Ulbrich, I., Crounse, J., de Foy, B., Dunlea, E., Aiken, A., Knapp, D., Weinheimer,
376 A., Campos, T., Wennberg, P., Jimenez, J.: Investigation of the sources and processing of
377 organic aerosol over the Central Mexican Plateau from aircraft measurements during
378 MILAGRO. Atmos. Chem. Phys. 10(12), 5257 -5280, 2010.

379 Draxler, R.R. and Hess, G.D.: An overview of the HYSPLIT_4 modelling system for
380 trajectories, dispersion, and deposition. Australian Meteorological Magazine, 47, 295-308,
381 1998.

382 Duan, J., Huang, R.-J., Lin, C., Dai, W., Wang, M., Gu, Y., Wang, Y., Zhong, H., Zheng, Y., Ni,
383 H., Dusek, U., Chen, Y., Li, Y., Chen, Q., Worsnop, D.R., O'Dowd, C.D., Cao, J.J.:
384 Distinctions in source regions and formation mechanisms of secondary aerosol in Beijing
385 from summer to winter. Atmos. Chem. Phys. 19, 10319–10334, 2019.

386 Duan, J., Huang, R., Li, Y., Chen, Q., Zheng, Y., Chen, Y., Lin, C., Ni, H., Wang, M.,
387 Ovadnevaite, J., Ceburnis, D., Chen, C., Worsnop, D.R., Hoffmann, T., O'Dowd, C., Cao,
388 J.J.: Summertime and wintertime atmospheric processes of secondary aerosol in Beijing.
389 Atmos. Chem. Phys. 20, 3793–3807, 2020.

390 Duan, J., Huang, R.-J., Gu, Y., Lin, C., Zhong, H., Wang, Y., Yuan W., Ni, H., Yang, L., Chen,
391 Y., Worsnop, D., O'Dowd, C.: The formation and evolution of secondary organic aerosol
392 during summer in Xi'an: Aqueous phase processing in fog-rain days. Sci. Total Environ. 756

(20), 144077, 2021.

Du, H., Li, J., Chen, X., Wang, Z., Sun, Y., Fu, P., Li, J., Gao, J., and Wei, Y.: Modeling of aerosol property evolution during winter haze episodes over a megacity cluster in northern China: roles of regional transport and heterogeneous reactions of SO2, Atmos. Chem. Phys., 19, 9351–9370, 2019.

Elser, M., Huang, R., Wolf, R., Slowik, J., Wang, Q., Canonaco, F., Li, G., Bozzetti, C., Daellenbach, K., Huang, Y., Zhang, R., Li, Z., Cao, J., Baltensperger, U., El-Haddad, I., Prévôt, A.: New insights into $PM_{2.5}$ chemical composition and sources in two major cities in China during extreme haze events using aerosol mass spectrometry. Atmos. Chem. Phys. 16, 3207–3225, 2016.

Feng, T., Bei, N., Zhao, S., Wu, J., Li, X., Zhang, T., Cao, J., Zhou, W., Li, G.: Wintertime nitrate formation during haze days in the Guanzhong basin, China: a case study. Environ. Pollut., 243, 1057-1067, 2018.

Fierce, L., Bond, T. C., Bauer, S. E., Mena, F., and Riemer, N.: Black carbon absorption at the global scale is affected by particle-scale diversity in composition, Nat. Commun., 7, 12361, 2016.

Fröhlich, R., Cubison, M., Slowik, J., Bukowiecki, N., Prévôt, A., Baltensperger, U., Schneider, J., Kimmel, J., Gonin, M., Rohner, U., Worsnop, D., Jayne, J.: The ToF-ACSM: a portable aerosol chemical speciation monitor with TOFMS detection, Atmos. Meas. Tech., 6(11), 3225-3241, 2013.

Gunsch, M. J., May, N. W., Wen, M., Bottenus, C. L. H., Gardner, D. J., VanReken, T. M., Bertman, S. B., Hopke, P. K., Ault, A. P., and Pratt, K. A.: Ubiquitous influence of wildfire emissions and secondary organic aerosol on summertime atmospheric aerosol in the forested Great Lakes region, Atmos. Chem. Phys., 18, 3701–3715, 2018.

Guo, J., Zhou, S., Cai, M., Zhao, J., Song, W., Zhao, W., Hu, W., Sun, Y., He, Y., Yang, C., Xu, X., Zhang, Z., Cheng, P., Fan, Q., Hang, J., Fan, S., Wang, X., and Wang, X.: Characterization of submicron particles by time-of-flight aerosol chemical speciation monitor (ToF-ACSM) during wintertime: aerosol composition, sources, and chemical processes in Guangzhou, China, Atmos. Chem. Phys., 20, 7595–7615, 2020.

Hao, J., Lv, Z., Chu, B., Wu, S., Zhao, Z., et al.: Characterization, Experimental study, and Modeling of Atmospheric Secondary Organic Aerosol [M]. Beijing: Science Press., 83-94, 2015.

Huang, Y., Li, L., Li, J., Wang, X., Chen, H., Chen, J., Yang, X., Gross, D., Wang, H., Qiao, L., Chen, C.: A case study of the highly time-resolved evolution of aerosol chemical and optical properties in urban Shanghai, China. Atmos. Chem. Phys. 13, 3931–3944, 2013.

Huang, R., Zhang, Y., Bozzetti, C., Ho, K., Cao, J., Han, Y., Daellenbach, K.R., Slowik, J.G., Platt, S.M., Canonaco, F.: High secondary aerosol contribution to particulate pollution during haze events in China. Nature 514 (7521), 218-222, 2014.

Huang, R.-J., Wang, Y., Cao, J., Lin, C., Duan, J., Chen, Q., Li, Y., Gu, Y., Yan, J., Xu, W., Fröhlich, R., Canonaco, F., Bozzetti, C., Ovadnevaite, J., Ceburnis, D., Canagaratna, M.R., Jayne, J., Worsnop, D.R., El-Haddad, I., Prévôt, A.S.H., O'Dowd, C.D.: Primary emissions versus secondary formation of fine particulate matter in the most polluted city (Shijiazhuang) in North China. Atmos. Chem. Phys. 19, 2283–2298, 2019.

Huang, X., He, L., Xue, L., Sun, T., Zeng, L., Gong, Z. H., Hu, M., and Zhu, T.: Highly time-resolved chemical characterization of atmospheric fine particles during 2010 shanghai world expo, Atmos. Chem. Phys., 12, 4897–4907, 2012.

Huang, X., Xue, L., Tian, X., Shao, W., Sun, T., Gong, Z., Ju, W., Jiang, B., Hu, M., and He, L.: Highly time-resolved carbonaceous aerosol characterization in yangtze river delta of china: Composition, mixing state and secondary formation, Atmos. Environ., 64, 200–207, 2013.

Huang, X., Ding, A., Wang, Z., Ding, K., Gao, J., Chai, F., Fu, C.: Amplified transboundary transport of haze by aerosol–boundary layer interaction in China. Nature Geosci., 13, 428-434, 2020.

Hu, W., Hu, M., Yuan, B., Jimenez, J., Tang, Q., Peng, J., Hu, W., Shao, M., Wang, M., Zeng, L., Wu, Y., Gong, Z., Huang, X., and He, L.: Insights on organic aerosol aging and the inflfluence of coal combustion at a regional receptor site of central eastern china, Atmos. Chem. Phys., 13, 10095–10112, 2013.

Ji, Y., Qin, X., Wang, B., Xu, J., Shen, J., Chen, J., Huang, K., Deng, C., Yan, R., Xu, K., and Zhang, T.: Counteractive effects of regional transport and emission control on the formation of fine particles: a case study during the Hangzhou G20 summit, Atmos. Chem. Phys., 18, 13581–13600, 2018.

Kim, H., Zhang, Q., and Heo, J.: Influence of intense secondary aerosol formation and long-range transport on aerosol chemistry and properties in the Seoul Metropolitan Area during spring time: results from KORUS-AQ, Atmos. Chem. Phys., 18, 7149–7168, 2018.

Kindap, T., Unal, A., Chen, S., Hu, Y., Odman, M., Karaca, M.: Long-range aerosol transport from Europe to Istanbul, Turkey. Atmos, Environ., 40(19), 3536-3547, 2006.

Lee, B; Li, Y; Yu, J.; Louie, P.; Chan, C.: Physical and chemical characterization of ambient aerosol by HR-ToF-AMS at a suburban site in Hong Kong during springtime 2011. J. GEOPHYS. RES., 118(15), 8625–8639, 2013.

Lei, Y., Zhang, Q., He, K., Streets, D.: Primary anthropogenic aerosol emission trends for China, 1990–2005. Atmos. Chem. Phys. 11, 931–954, 2011.

Lelieveld, J., Evans, J. S., Fnais, M., Giannadaki, D., and Pozzer, A.: The contribution of outdoor air pollution sources to premature mortality on a global scale, Nature, 525, 367–371, 2015.

Li, Y., Lee, B., Su, L., Fung, J., Chan, C.: Seasonal characteristics of fine Journal Pre-proof Journal Pre-proof 23 particulate matter (PM) based on high -resolution time -of-flight aerosol mass spectrometric (HR -ToF -AMS) measurements at the HKUST Supersite in Hong Kong.

Atmos. Chem. Phys. 15(1), 37 -53, 2015.

Li, H., Cheng, J., Zhang, Q., Zheng, B., Zhang, Y., Zheng, G., He, K.: Rapid transition in winter aerosol composition in Beijing from 2014 to 2017: response to clean air actions. Atmos. Chem. Phys. 19, 11485–11499, 2019.

Li, J. and Han, Z.: A modeling study of severe winter haze events in Beijing and its neighboring regions, Atmos. Res., 170, 87–97, 2016.

Li, J., Du, H., Wang, Z., Sun, Y., Yang, W., Li, J., Tang, X., and Fu, P.: Rapid formation of a severe regional winter haze episode over a mega-city cluster on the North China Plain, Environ. Pollut., 223, 605–615, 2017.

Li, J., Liu, Z., Cao, L., Gao, W., Yan, Y., Mao, J., Zhang, X., He, L., Xin, J., Tang, G., Ji, D., Hu, B., Wang, L., Wang, Y., Dai, L., Zhao, D., Du, W., Wang, Y.: Highly time-resolved chemical characterization and implications of regional transport for submicron aerosols in the North China Plain, Sci. Total. Environ., 705, 135803, 2021.

Li, J., Cao, L., Gao, W., He, L., Yan, Y., He, Y., Pan, Y., Ji, D., Liu, Z., and Wang, Y.: Seasonal variations in the highly time-resolved aerosol composition, sources and chemical processes of background submicron particles in the North China Plain, Atmos. Chem. Phys., 21, 4521–4539, 2021.

Lin, C., Huang, R.-J., Duan, J., Zhong, H., Xu, W., Wu, Y., Zhang, R.: Large contribution from worship activities to the atmospheric soot particles in northwest China. Environ. Pollut. 299(15), 118907, 2022.

Liu, P., Zhang, Y., Wu, T., Shen, Z., Xu, H.: Acid -extractable heavy metals in PM2.5 over Xi'an, China: seasonal distribution and meteorological influence. Environ Sci Pollut Res. 26 (33), 34357 -34367, 2019.

Liu, Q., Liu, D., Wu, Y., Bi, K., Gao, W., Tian, P., Zhao, D., Li, S., Yu, C., Tang, G., Wu, Y., Hu, K., Ding, S., Gao, Q., Wang, F., Kong, S., He, H., Huang, M., and Ding, D.: Reduced volatility of aerosols from surface emissions to the top of the planetary boundary layer, Atmos. Chem. Phys., 21, 14749–14760, 2021.

Liu, Z., Gao, W., Yu, Y., Hu, B., Xin, J., Sun, Y., Wang, L., Wang, G., Bi, X., Zhang, G., Xu, H., Cong, Z., He, J., Xu, J., and Wang, Y.: Characteristics of $PM_{2.5}$ mass concentrations and chemical species in urban and background areas of China: emerging results from the CARE-China network, Atmos. Chem. Phys., 18, 8849–8871, 2018.

Middlebrook, A., Bahreini, R., Jimenez, J., Canagaratna, M.: Evaluation of composition-dependent collection efficiencies for the aerodyne aerosol mass spectrometer using field data. Aerosol Sci. Tech. 46(3), 258-271, 2012.

Moffet, R. C. and Prather, K. A.: In-situ measurements of the mixing state and optical properties of soot with implications for radiative forcing estimates. P. Natl. Acad. Sci., 106, 11872–11877, 2009.

Ng, N., Canagaratna, M., Zhang, Q., Jimenez, J., Tian, J., Ulbrich, I., Kroll, J., Docherty, K., Chhabra, P., Bahreini, R., Murphy, S., Seinfeld, J., Hildebrandt, L., Donahue, N., DeCarlo, P., Lanz, V., Prévôt, A., Dinar, E., Rudich, Y. and Worsnop, D.: Organic aerosol components observed in Northern Hemispheric datasets from Aerosol Mass Spectrometry. Atmos. Chem. Phys., 10, 4625–4641, 2010.

Paatero, P. and Tapper, U.: Positive Matrix Factorization: a nonnegative factor model with optimal utilization of error estimates of data values. Environmetrics. 5(2), 111-126, 1994.

Paatero, P.: Least squares formulation of robust non-negative factor analysis. Chemom. Intell. Lab. 37(1), 23-35, 1997.

Paatero, P.: The multilinear engine: a table-driven, least squares program for solving multilinear problems, including the n-way parallel factor analysis model. J. Comput. Graph. Stat. 8(4), 854-888, 1999.

Pandis, N., Harley, R., Cass, G., Seinfeld, J.: Secondary organic aerosol formation and transport. Atmos. Environ., 26(13), 2269-2282, 1992.

Pu, W., Zhao, X., Shi, X., Ma, Z., Zhang, X., Bo, Y.: Impact of long-range transport on aerosol properties at a regional background station in Northern China. Atmos. Res., 153, 489-499, 2015.

Reyes-Villegas, E., Green, D. C., Priestman, M., Canonaco, F., Coe, H., Prévôt, A. S. H., and Allan, J. D.: Organic aerosol source apportionment in London 2013 with ME-2: exploring the solution space with annual and seasonal analysis, Atmos. Chem. Phys., 16, 15545–15559, 2016.

Riemer, N. and West, M.: Quantifying aerosol mixing state with entropy and diversity measures, Atmos. Chem. Phys., 13, 11423–11439, 2013.

Salvador, P., Artinano, B., Querol, X., Alastuey, A.: A combined analysis of backward trajectories and aerosol chemistry to characterize long-range transport episodes of particulate matter. The Madrid air basin, a case study. Sci. Total Environ., 390, 495-506, 2008.

Schichtel, B., Gebhart, K., Barna, M., Malm, W.: Association of air mass transport patterns and particulate sulfur concentrations at Big Bend National Park, Texas. Atmos. Environ., 40, 992-1006, 2006.

Shen, Z., Cao, J., Liu, S., Zhu, C., Wang, X., Zhang, T., Xu, H., Hu, T.: Chemical composition of PM10 and PM2.5 collected at ground level and 100 meters during a strong winter-time pollution episode in Xi'an, China. J. AIR WASTE MANAGE., 61, 1150−1159, 2011.

Srivastava, D., Favez, O., Perraudin, E., Villenave, E., & Albinet, A.: Comparison of measurement-based methodologies to apportion secondary organic carbon (SOC) in PM2.5: a review of recent studies. Atmosphere, 9(11), 452, 2018.

Sun, Y., Wang, Z., Fu, P., Yang, T., Jiang, Q., Dong, H., Li, J., Jia, J.: Aerosol composition, sources and processes during wintertime in Beijing, China. Atmos. Chem. Phys. 13, 4577–

4592, 2013.

Sun, C., Lee, B., Huang, D., Jie Li, Y., Schurman, M., Louie, P., Luk, C., Chan, C.: Continuous measurements at the urban roadside in an Asian megacity by Aerosol Chemical Speciation Monitor (ACSM): particulate matter characteristics during fall and winter seasons in Hong Kong. Atmos. Chem. Phys. 16(3), 1713 -1728, 2016.

Sun, P., Nie, W., Chi, X., Huang, X., Ren, C., Xue, L., Shan, Y., Wen L., Li, H., Chen, T., Qi, Y., Gao, J., Zhang, Q., and Ding, A.: Aircraft study of secondary aerosols in long-range transported air masses from the North China Plain by a mid-latitude cyclone. Journal of Geophysical Research: Atmospheres, 127, e2021JD036178, 2022.

Tang, L., Eugensson, M., Sjöberg, K., Wichmann, J.: Estimation of the long-range transport contribution from secondary inorganic components to urban background PM10 concentrations in south-western Sweden during 1986–2010. Atmos. Environ., 89, 93-101, 2014.

Tang, G., Zhang, J., Zhu, X., Song, T., Münkel, C., Hu, B., Schäfer, K., Liu, Z., Zhang, J., Wang, L., Xin, J., Suppan, P., and Wang, Y.: Mixing layer height and its implications for air pollution over Beijing, China, Atmos. Chem. Phys., 16, 2459–2475, 2016.

Tie, X., Huang, R.-J., Dai, W., Cao, J., Long, X., Su, X., Zhao, S., Wang, Q., Li, G.: Effect of heavy haze and aerosol pollution on rice and wheat productions in China. Sci. Rep. 6(1), 29612, 2016.

Tie, X. and Cao, J.: Aerosol pollution in China: Present and future impact on environment. Particuology. 7(6), 426-431, 2009.

Updyke, K., Nguyen, T., Nizkorodov, S.: Formation of brown carbon via reactions of ammonia with secondary organic aerosols from biogenic and anthropogenic precursors. Atmos. Environ., 63, 22-31, 2012.

Uno, I., Eguchi, K., Yumimoto, K., Takemura, T., Shimizu, A., Uematsu, M., Liu, Z., Wang, Z., Hara, Y., and Sugimoto, N.: Asian dust transported one full circuit around the globe, Nat. Geosci., 2, 557–560, 2009.

Wang, Y., Huang, R., Ni, H., Chen, Y., Wang, Q., Li, G., Tie, X., Shen, Z., Huang, Y., Liu, S., Dong, W., Xue, P., Frohlich, R., Canonaco, F., Elser, M., Daellenbach, K., Bozzetti, C., El-Haddad, I., Prévôt, A., Canagaratna, M., Worsnop, D., Cao, J.: Chemical composition, sources and secondary processes of aerosols in Baoji city of northwest China. Atmos. Environ. 158, 128 -137, 2017.

Wang, H., Wang, Q., Gao, Y., Zhou, M., Jing, S., Qiao, L., Yuan, B., Huang, D., Huang, C., Lou, S., Yan, R., Gouw, J., Zhang, X., Chen, J., Chen, C., Tao, S., An, J., Li, Y.: Estimation of Secondary Organic Aerosol Formation During a Photochemical Smog Episode in Shanghai, China. Journal of Geophysical Research: Atmospheres. 125(7), e2019JD032033, 2020.

Wehner, B., Philippin, S., Wiedensohler, A., Scheer, V., and Vogt, R.: Variability of non-volatile fractions of atmospheric aerosol particles with traffic influence, Atmospheric Environment,

38, 6081–6090, 2004.

Wu, C., & Yu, J. Z.: Determination of primary combustion source organic carbon-toelemental carbon (OC/EC) ratio using ambient OC and EC measurements: secondary OC-EC correlation minimization method. Atmos. Chem. Phys., 16(8), 5453–5465, 2016.

Xu, J., Tao, J., Zhang, R., Cheng, T., Leng, C., Chen, J., Huang, G., Li, X., Zhu, Z.: Measurements of surface aerosol optical properties in winter of Shanghai. Atmos. Res. 109-110, 25-35, 2012.

Xu, J., Zhang, Q., Chen, M., Ge, X., Ren, J., Qin, D.: Chemical composition, sources, and processes of urban aerosols during summertime in northwest China: insights from high-resolution aerosol mass spectrometry. Atmos. Chem. Phys., 14, 12593–12611, 2014.

Xu, W., Xie, C., Karnezi, E., Zhang, Q., Wang, J., Pandis, S., Ge, X., Zhang, J., An, J., Wang, Q., Zhao, J., Du, W., Qiu, Y., Zhou, W., He, Y., Li, Y., Li, J., Fu, P., Wang, Z., Worsnop, D., Sun, Y.: Summertime aerosol volatility measurements in Beijing, China. Atmos. Chem. Phys. 19, 10205-10216, 2019.

Yang, Y. R., Liu, X. G., Qu, Y., Wang, J. L., An, J. L., Zhang, Y., and Zhang, F.: Formation mechanism of continuous extreme haze episodes in the megacity Beijing, China, in January 2013, Atmos. Res., 155, 192–203, 2015.

Zhang, K., Leeuw, G., Yang, Z., Chen, X., Su, X., Jiao, J.: Concentrations Using VIIRS-Derived AOD in the Guanzhong Basin, China. Remote Sens., 11(22), 2679, 2019.

Zhang, Q., Shen, Z., Zhang, L., Zheng, Y., Ning, Z., Zhang, T., Lei, Y., Wang, Q., Li, G., Sun, J., Westerdahl, D., Xu, H., Cao, J.: Investigation of Primary and Secondary Particulate Brown Carbon in Two Chinese Cities of Xi'an and Hong Kong in Wintertime. Environ. Sci. Technol., 54, 7, 3803–3813, 2020.

Zhong, H., Huang, R., Duan, J., Lin, C., Gu, Y., Wang, Y., Li, Y., Zheng, Y., Chen, Q., Chen, Y., Dai, W., Ni, H., Chang, Y., Worsnop, D., Xu, W., Ovadnevaite, J., Ceburnis, D., O'Dowd, C.: Seasonal variations in the sources of organic aerosol in Xi'an, Northwest China: the importance of biomass burning and secondary formation. Sci. Total. Environ. 737, 139666, 2020.

Zhong, H., Huang, R., Lin, C., Xu, W., Duan, J., Gu, Y., Huang, W., Ni, H., Zhu, C., You, Y., Wu, Y., Zhang, R., Ovadnevaite, J., Ceburnis, D., O'Dowd, C.D..: Data for "Measurement report: On the contribution of long-distance transport to the secondary aerosol formation and aging", Zenodo [data set], https://doi.org/10.5281/zenodo.6446514, 2022.

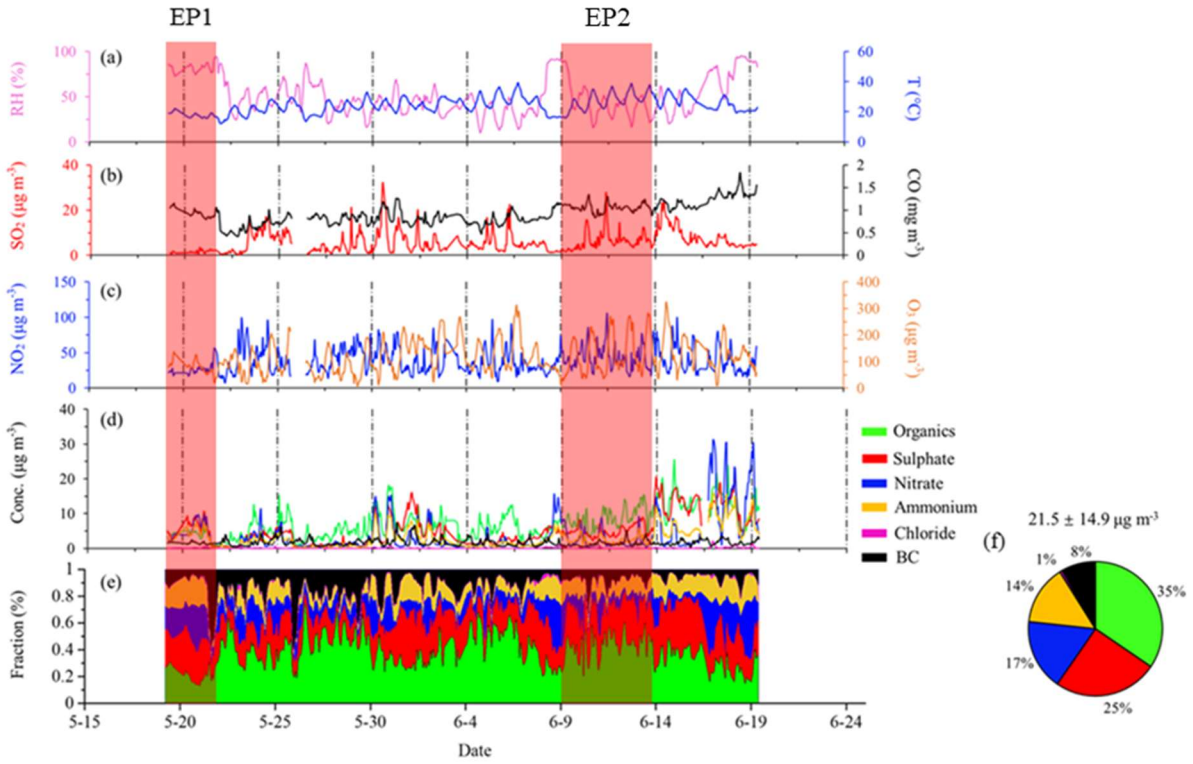

613

614 **Figure 1.** Time series of (a) relative humidity and temperature, (b, c) mass concentration of
615 SO_2, CO, NO_2 and O_3 (d, e) mass concentrations and fractional contributions of $PM_{2.5}$ (organics,
616 sulphate, nitrate, ammonium, chloride and BC) during the campaign period. Five pollution
617 episodes are observed during the entire campaign, and they are detailly analyzed by HYSPLIT
618 model and showed in Fig. S3. EP1 and EP2 (shaded) are the only two pollution episodes caused
619 by continuous transport from the BTH transport and the urban GZB transport, respectively.
620 Therefore, they are selected for further discussion.

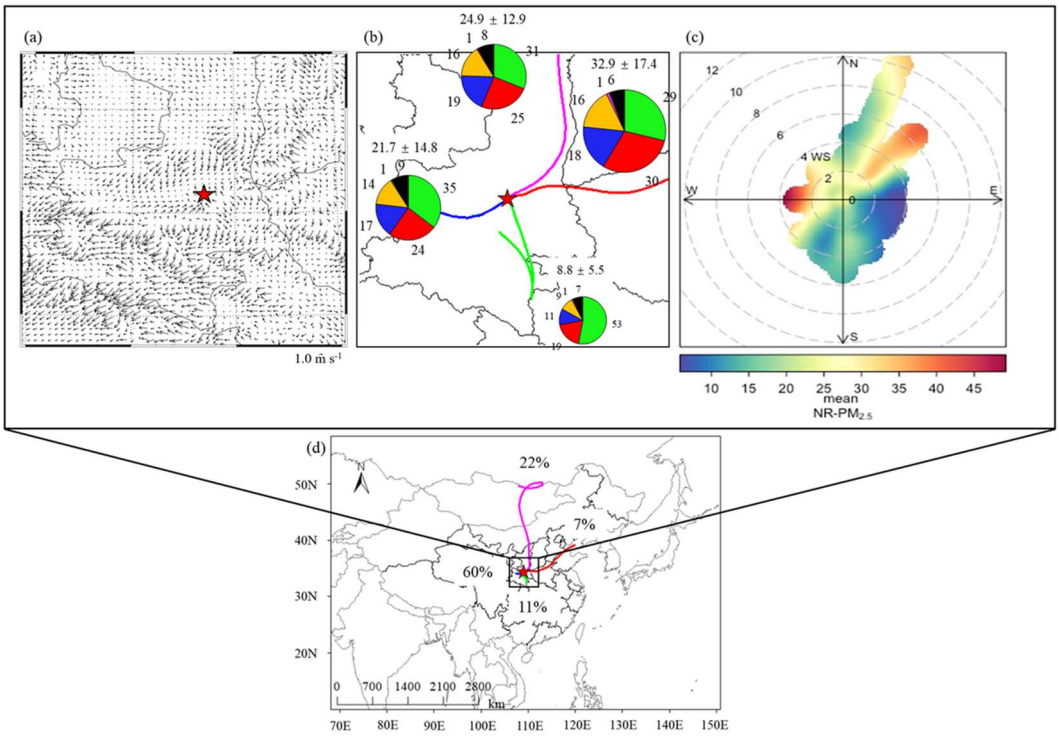

Figure 2. (a) Wind field, (b, d) backward trajectory and (c) wind rose results during the campaign. There are four transport clusters observed during the campaign, which are the northern China transport (the north cluster, magenta, 22% of observing days) and the BTH transport (the east cluster, red, 7% of observing days), the western GZB transport (the west cluster, blue, 60% of observing days) and the southern GZB transport (the south cluster, green, 11% of observing days).

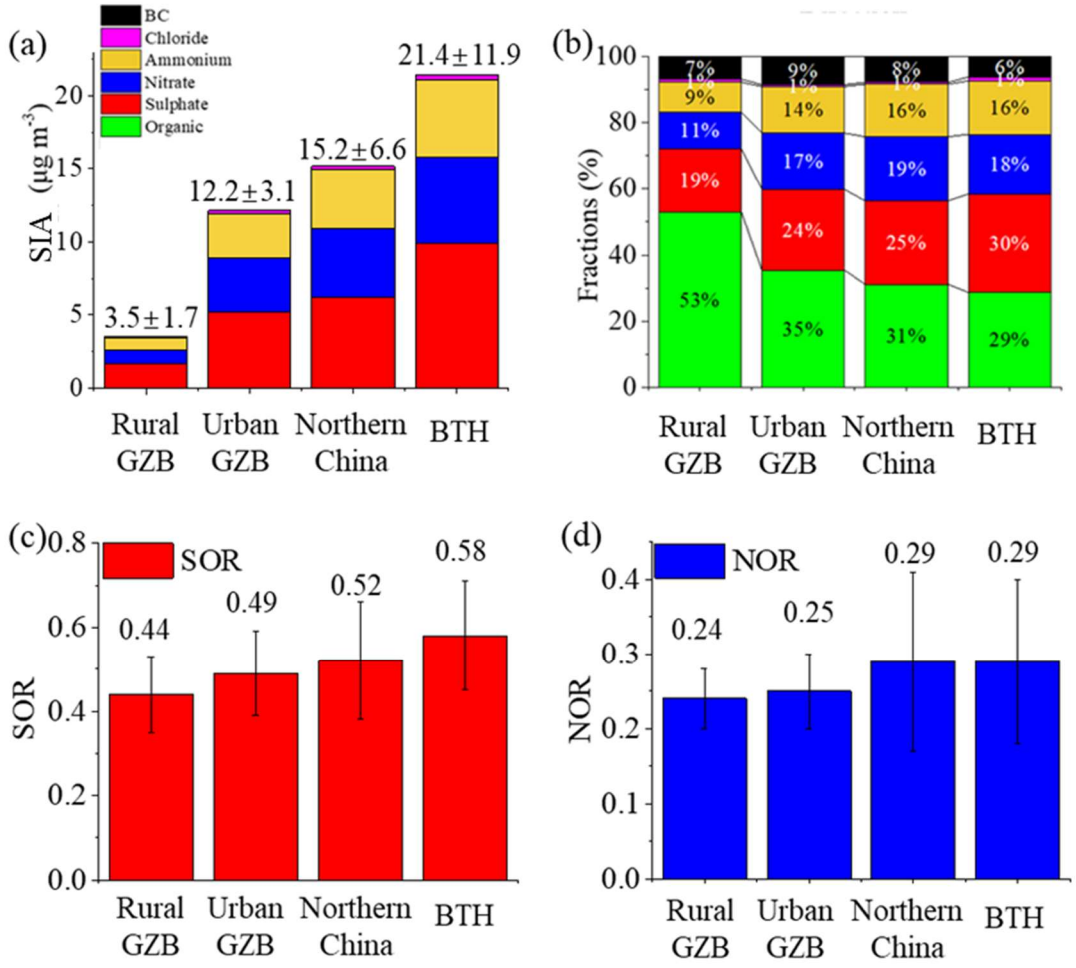

628

629 **Figure 3.** The comparison of (a) the mass concentration of SIA, (b) chemical fractions of $PM_{2.5}$,
630 (c) sulphur oxidation ratio (SOR) and (d) nitrogen oxidation ratio (NOR) in four transport
631 sectors.

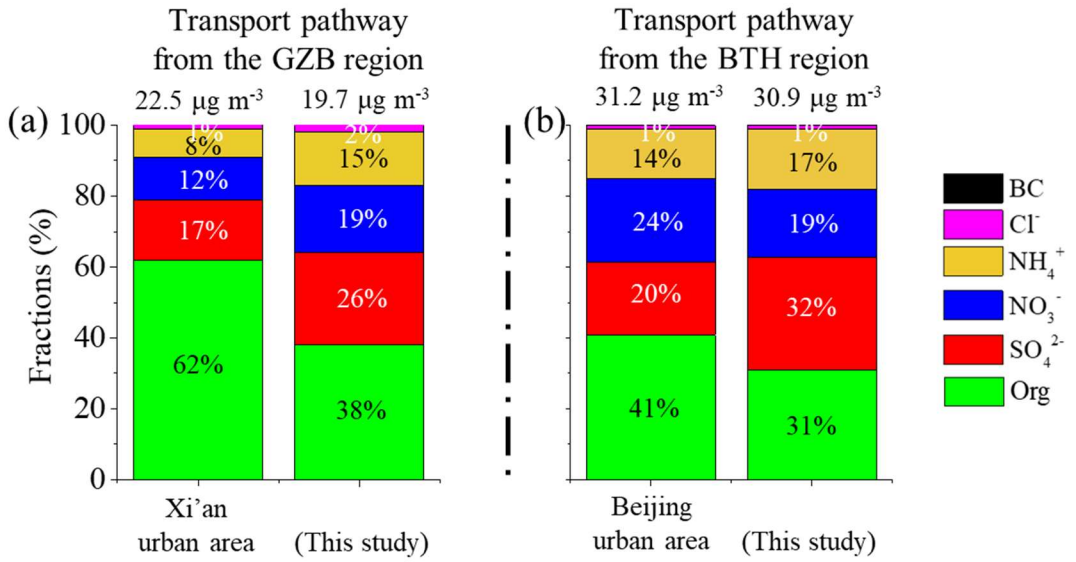

632

633 **Figure 4.** Chemical composition of the observing results which were long-term observation and
634 were right on the transport route of the BTH transport and the GZB transport, including the
635 Beijing urban area (Xu et al., 2019), the Xi'an urban area (Duan et al., 2021), the BTH transport
636 in this study (East transport) and the urban GZB transport in this study (West transport).

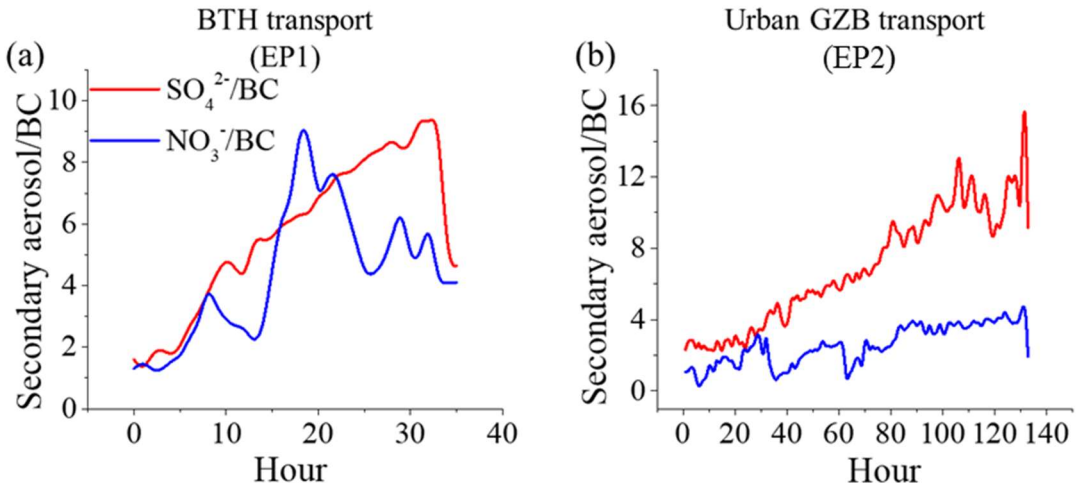

637

638 **Figure 5.** The relationship between production of the secondary inorganic aerosol and transport
639 duration in the pollution episodes. EP1 and EP2 represented the pollution episodes caused by
640 the BTH transport and the urban GZB transport, respectively.

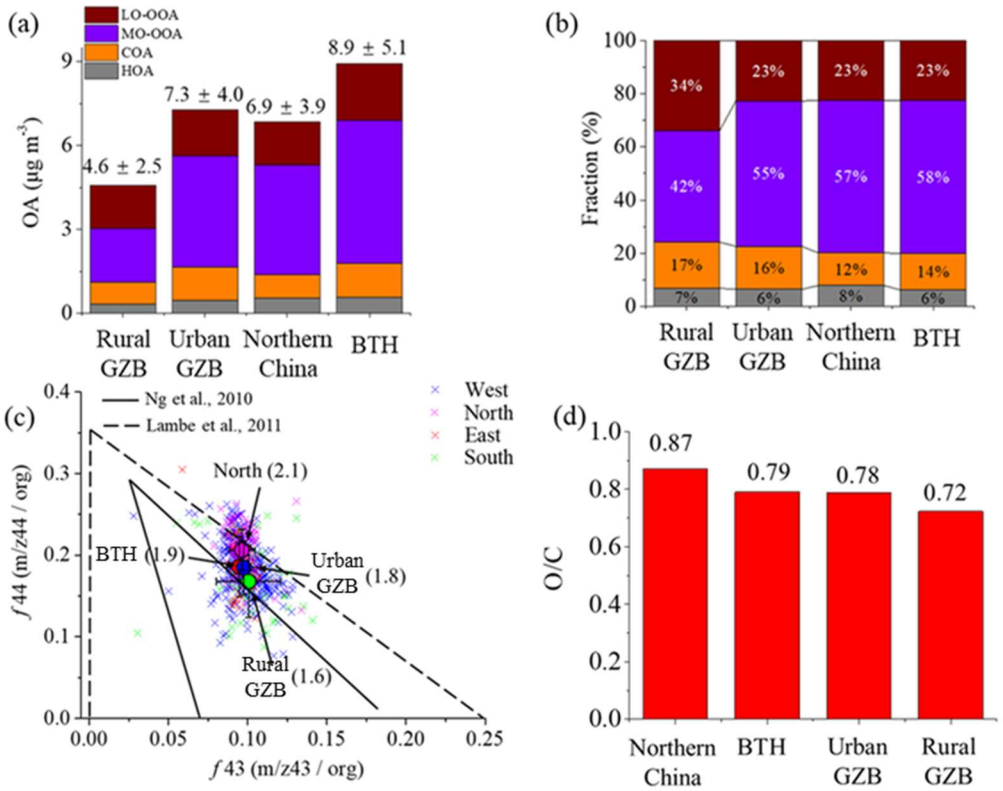

641

642 **Figure 6.** The comparison of (a) the mass concentration and (b) fractions of organic aerosol. (c)
643 Scatter plot of *f*44 v.s. *f*43 in four transport directions. The triangle from Ng et al., (2010) and
644 Lambe et al., (2011) is drawn in solid line and dotted line, respectively. (d) The O/C ratio in four
645 transport directions.

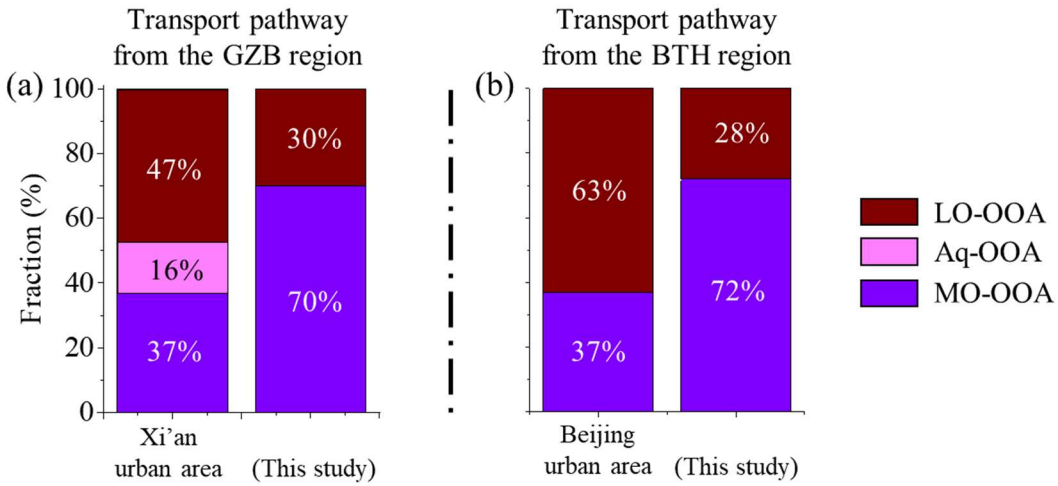

646

647 **Figure 7.** OA factors of the observing results which were long-term observation and were right
648 on the transport route of the BTH transport and the GZB transport, including the Beijing urban
649 area (Xu et al., 2019), the Xi'an urban area (Duan et al., 2021), the BTH transport in this study

(East transport) and the urban GZB transport in this study (West transport).

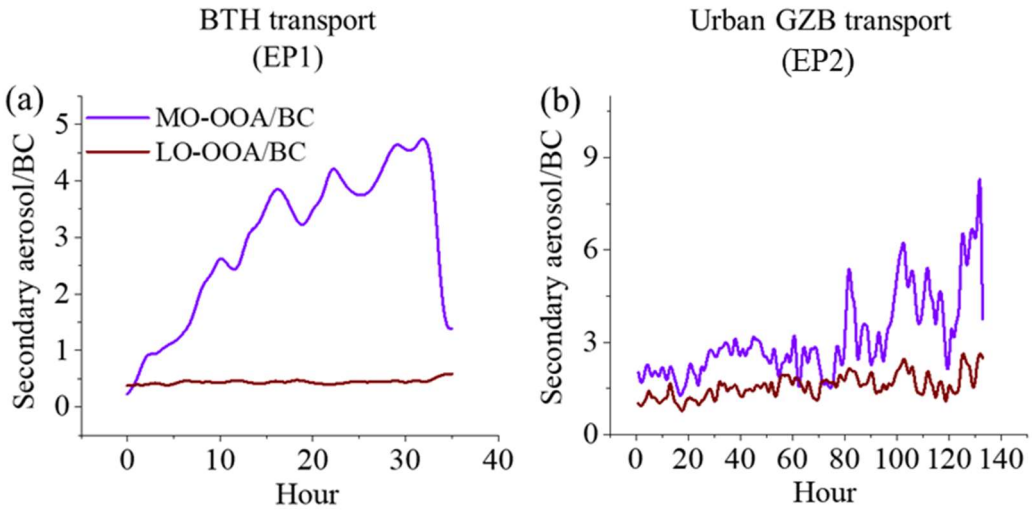

Figure 8. The relationship between production of the secondary organic aerosol and transport duration in the pollution episodes. EP1 and EP2 represented the pollution episodes caused by the BTH transport and the urban GZB transport, respectively.